LAWRENCE
LIVERMORE
NATIONAL
LABORATORY

LLNL-JRNL-402714

Wear Resistant Amorphous and Nanocomposite Coatings

O. Racek

April 4, 2008

Metallurgical and Materials Transactions

Disclaimer

This document was prepared as an account of work sponsored by an agency of the United States government. Neither the United States government nor Lawrence Livermore National Security, LLC, nor any of their employees makes any warranty, expressed or implied, or assumes any legal liability or responsibility for the accuracy, completeness, or usefulness of any information, apparatus, product, or process disclosed, or represents that its use would not infringe privately owned rights. Reference herein to any specific commercial product, process, or service by trade name, trademark, manufacturer, or otherwise does not necessarily constitute or imply its endorsement, recommendation, or favoring by the United States government or Lawrence Livermore National Security, LLC. The views and opinions of authors expressed herein do not necessarily state or reflect those of the United States government or Lawrence Livermore National Security, LLC, and shall not be used for advertising or product endorsement purposes.

Wear resistant amorphous and nanocomposite coatings

Ondrej Racek
Caterpillar Inc., Peoria, IL, USA

Keywords: coatings, wear/wear resistance, nanocomposites, HVOF

Abstract

Glass forming materials (critical cooling rate $<10^4 K.s^{-1}$) are promising for their high corrosion and wear resistance. During rapid cooling, the materials form an amorphous structure that transforms to nanocrystalline during a process of devitrification. High hardness (HV 1690) can be achieved through a controlled crystallization. Thermal spray process has been used to apply coatings, which preserves the amorphous/nanocomposite structure due to a high cooling rate of the feedstock particles during the impact on a substrate. Wear properties have been studied with respect to process conditions and feedstock material properties. Application specific properties such as sliding wear resistance have been correlated with laboratory tests based on instrumented indentation and scratch tests.

Introduction

Amorphous materials provide excellent corrosion resistance [1]. It is possible to form a nanocrystalline structure through the process of devitrification and achieve high hardness up to HV 1690 (100 g load) [2]. Compositions with a low critical cooling rate that can be produced in a large scale were developed at Idaho National Laboratory under DARPA and DOE programs [2, 3]. Other materials, for example $Fe_{64}Mo_{14}C_{15}B_7$, have been reported cast as ingots of up to 2.5 mm in diameter [4]. The materials developed at Idaho National Laboratory [2] and at the University of Virginia [4] are characterized by high boron or molybdenum content, respectively.

Thermal spray processes are suitable for amorphous material deposition due to the rapid cooling after impact of feedstock particles. To form an amorphous coating, material needs to be deposited either through a process that causes minimal melting or a process that causes a high degree of melting but the material is cooled fast enough after impact to form amorphous structure. Thermal spraying via high-velocity oxygen fuel (HVOF) process can achieve both conditions by suitable setting of parameters such as fuel and oxygen flows. In some instances, complete melting of particles during the thermal spray processing can increase the amount of amorphous phase [3].

Nanocrystalline materials have unique properties that are not attainable by conventional materials. For example, high hardness combined with ductility can be achieved in nanocrystalline copper [5]. The exceptional mechanical properties arise due to deformation mechanisms such as dislocation nucleation at the grain boundaries and sliding of grain boundaries. The most significant change in deformation mechanisms appears, however, when the grain size is less than 100 nm [6]. Nanocrystalline materials have been shown to provide a superior wear resistance [7], although ultra-fine grain size may cause excessive decomposition of carbides during the deposition process and therefore decrease the benefit of enhanced mechanical properties through nano-sized grains [8].

Materials and Methods

Feedstock and HVOF deposition process

The materials investigated in the present study are listed in Table 1. The exact compositions of the materials other than SAM2X5 and SAM1651 are confidential and will not be disclosed in the present study. The SAM materials are predominantly amorphous and are designed specifically for high corrosion resistance. The SAM materials development and corrosion testing was sponsored by Defense Advanced Projects Agency (DARPA), Defense Science Office (DSO), and the United States Department of Energy (DOE) Office of Civilian and Radioactive Waste Management (OCRWM). The corrosion resistance has been reported elsewhere [1]. Two additional materials, designated as SHS9192 and CATXP have a sub-micron grain size and are hard abrasion resistant materials. The Nanosteel Company, Providence, RI, supplied the fine-grained/amorphous materials to Caterpillar Inc. for testing. The wear behavior of the SHS 9172, CATXP, and SAM2X5 materials is compared to a "standard" chrome carbide-nickel cermet coating, 80% carbide 20% binder.

The coatings were deposited using a Praxair JP 5000 HVOF torch equipped with a 4" barrel. The deposition parameters are listed in Table 2. The coatings were ground to about 200μm thickness for the sliding wear test.

Table 1 List of feedstock materials

Feedstock materials													
		Fe	Cr	Mn	Mo	W	B	C	Si	Ni	Nb	Y	
SHS 9172*	Fine-grained	bal	<25	<3	<6	<15	<5	<4	<2	-	<12		wt.%
CATXP*	Fine-grained	bal	<25	<5	<10	<10	<5	<2	<2	<10	-		wt.%
SAM2X5	Amorphous	49.7	18.1	1.9	7.4	1.6	15.2	3.8	2.4	-	-	2	at.%
SAM1651	Amorphous	48	15		14		6	15					at.%
CrC-NiCr*	Cermet	-	69.3	-	-	-	-	10.7	-	20	-		wt.%

*Approximate composition, exact composition is proprietary

Table 2 HVOF deposition parameters

HVOF parameters (units)	
Kerosene fuel (slph)	25.7
Oxygen (slpm)	873
Surface speed (mm/s)	1990
Standoff (mm)	330*

One SAM2X5 run also at 356 mm

Sliding wear test

Lubricated sliding wear test was performed on flat coated and ground samples against a 6 mm diameter Si_3N_4 pin, Figure 1. The length of the pin that is in contact with the specimen is 12 mm. The test parameters are listed in Table 3. The coefficient of friction was monitored through the duration of the test. The volume of removed material, V, was measured after the test using contact profilometry and the Archard wear coefficient calculated as $K=V/PS$, where P is the normal force and S is the sliding distance. If the coefficient of friction is constant the Archard coefficient is proportional to the volume loss per unit of dissipated energy.

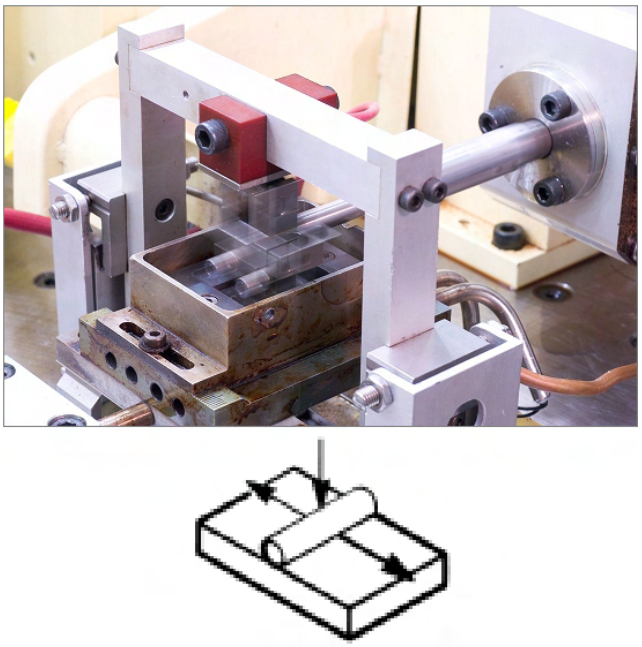

Figure 1 Reciprocating sliding wear test rig

Table 3 Sliding wear test conditions

Temperature	125	°C
Stroke	8.86	mm
Frequency	44	Hz
Sliding velocity	0.78	m/s
Initial Load	200	N
Lubricant	Fully formulated 15W-40	

Microstructure and indentation measurement

The microstructure was characterized using a scanning electron microscope LEO 1550 equipped with a field emission gun. The Vickers microhardness was measured with a LECO MHT series 200 instrument. Depth-sensitive micro-indentation (instrumented indentation) was conducted using a CSEM Micro Combi Tester with a Vickers indenter. The instrumented indentation test was performed in multiple loading-unloading where the maximum load increased in every cycle.

Analysis of the energy dissipation during wear is an approach to quantify wear damage, which has been demonstrated for fretting wear [9]. A relation of the indentation work to the wear properties has been reported for the cavitation resistance of a NiTi shape memory alloy. The wear coefficient was related to the ratio of the indentation work and the unrecovered depth after load removal and heating that induced a shape memory effect [10]. In the present study, the hysteresis of the un-loading and re-loading curve at each maximum load level was investigated.

Results

Microstructure

The microstructures of the SHS 9172 and CATXP feedstock particles typically consist of clearly crystalline phases, Figure 2a and b, which likely include $M_{23}(BC)_6$ and $M_7(BC)_3$, as described in published studies on similar materials [11]. A large number of the grains, especially in the CATXP material, are larger than 100 nm; therefore, these materials may not be strictly classified as nanocrystalline. The SHS 9172 and CATXP materials will be referred to as “fine-grained” for the purpose of the present investigation. The SAM2X5 material exhibits predominantly a structure without any evidence of a crystalline phase, Figure 2b. However, a small fraction of the particles, larger than about 50 microns in diameter, contain star-like carbides or borides and a phase that appears bright in SEM back-scattered electron imaging mode, which contains high content of molybdenum and chromium. It appears that the crystallization occurs due to a slower cooling rate within large particles, however, no systematic study has been performed to investigate this phenomenon. There were no grains observed in the SAM1651 feedstock material using SEM.

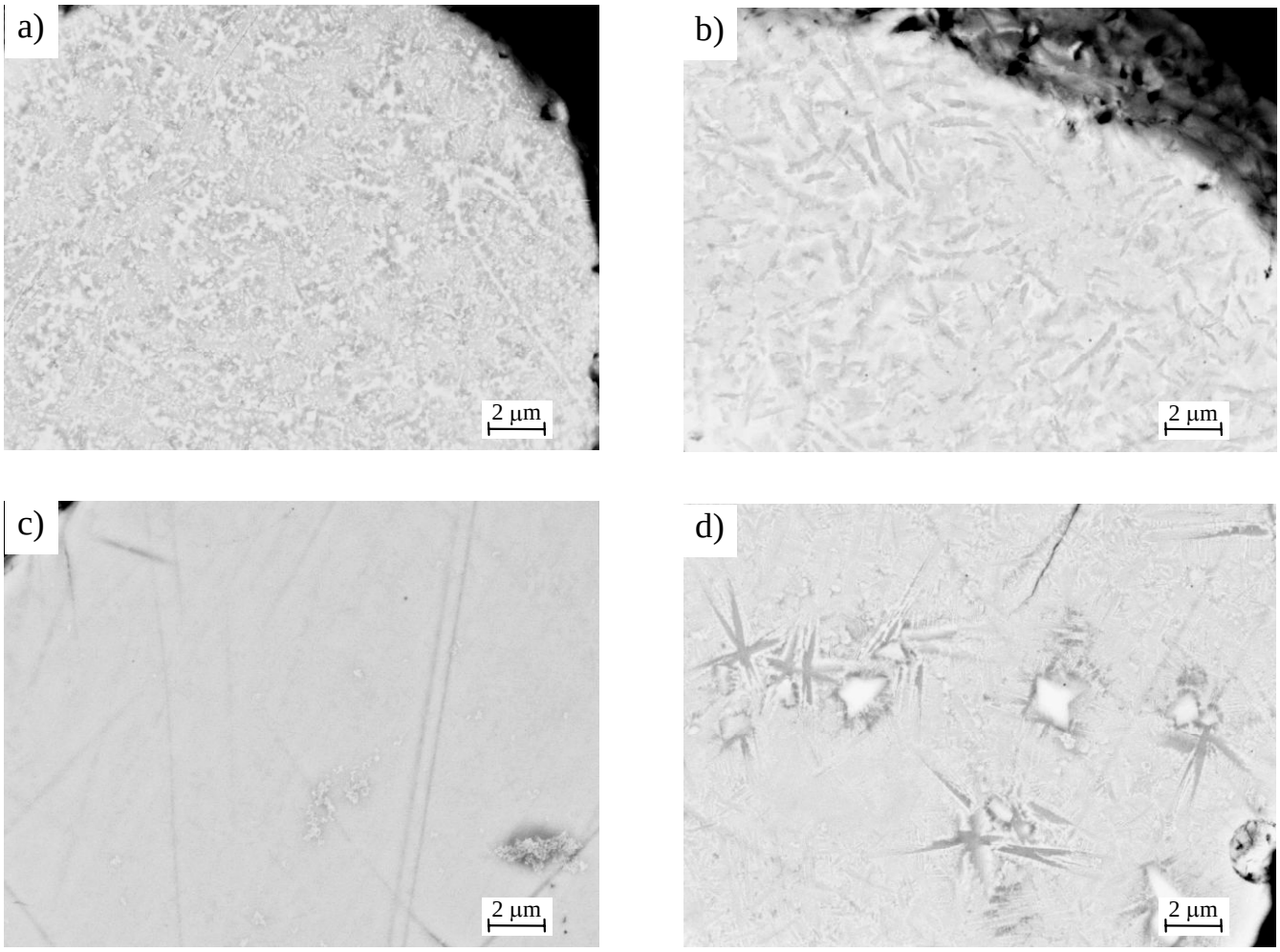

Figure 2 Feedstock particle microstructure; a) SHS 9172, b) CATXP, c) SAM2X5 no evidence of crystal structure, d) SAM2X5 crystallized phase

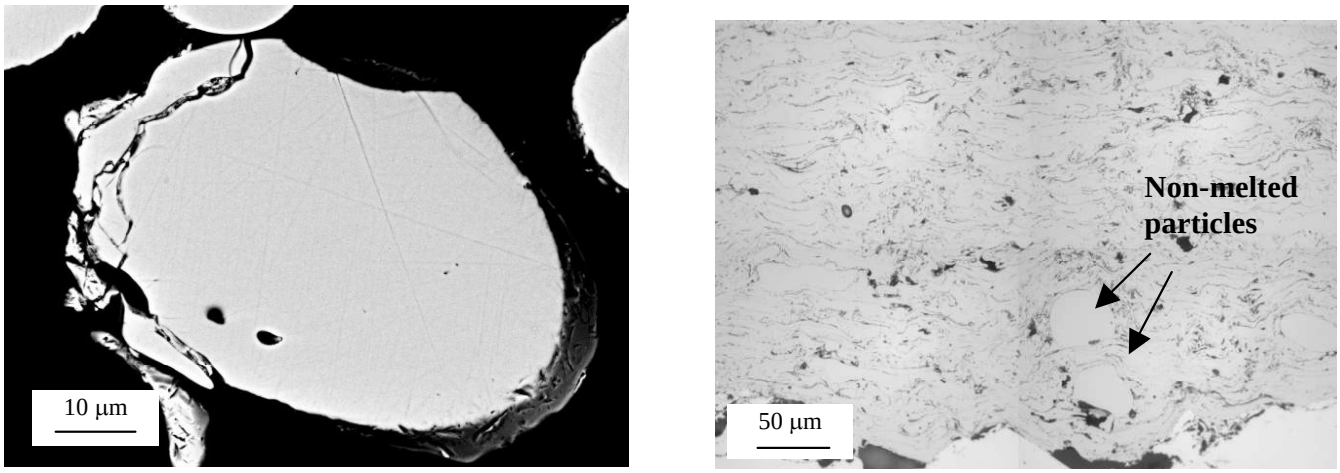

Figure 3 SAM1651; a) Feedstock particle, b) HVOF coating (optical micrograph)

During thermal spray processing the feedstock forms pancake shaped particles, splats that can be observed using light microscopy at about 200X magnification. Occasionally, non-melted particles are observed in the coating microstructure, Figure 3b. Non-melted particles can occur if the particle size is too large to be melted or if a particle traveled through colder marginal areas of a flame. Typically the non-melted particles within a coating microstructure are undesirable and should be minimized. HVOF coatings are dense; however, some inter-splat porosity exists as a result of imperfection in volume filling and cohesion between the splats, Figure 4a-d. The internal microstructure of the splats remains similar to the feedstock particles. The sub-micron-sized grains observed in the feedstock particles of SHS 9172 and CATXP are still present in the coating microstructure, Figure 4a, b. The internal splat microstructure of the SAM2X5 amorphous coating is not completely homogeneous, which may be a result of the residual crystalline phase. The CrC-NiCr coating consists of carbide particles that are held together by the binder Figure 4d.

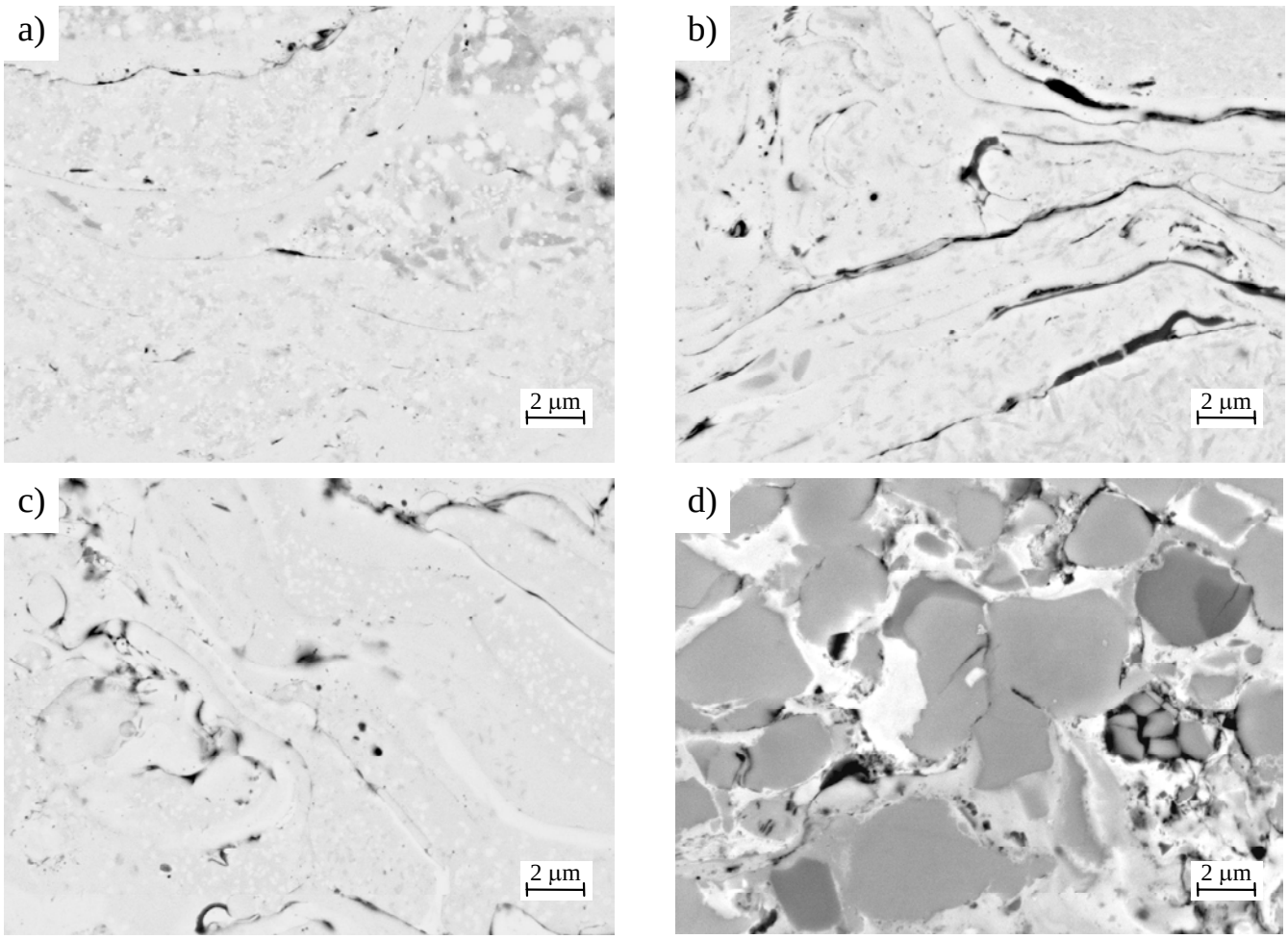

Figure 4 HVOF coating cross-section; a) SHS 9172, b) CATXP, c) Amorphous SAM2X5, d) CrC-NiCr

Hardness

The hardness of the coatings was determined in the plane of the coating (indentation on the cross-section) and in the normal direction to the coating (indentation on the ground and polished surface), Figure 5. The hardness of the CrC-NiCr coating in the normal direction is higher than the fine-grained/amorphous coatings. The amorphous coating SAM2X5 is softer than its fine-grained counterparts, which is consistent with the inverse Hall-Petch relationship observed in nanocrystalline materials [2].

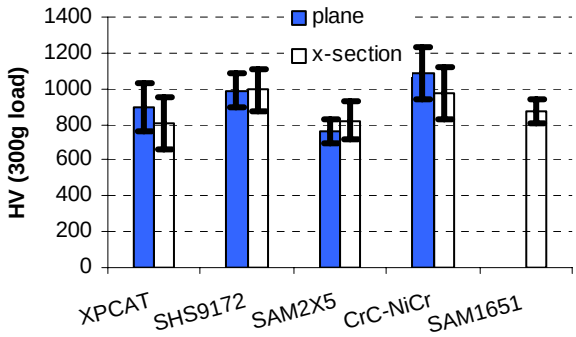

Figure 5 Coating hardness values in the normal and in-plane direction

Sliding Wear Test

The wear coefficient is expressed as volume of the material loss divided by the load and travel distance. Although the CrC-NiCr coating has higher Vickers hardness than the fine-grained/amorphous materials, the wear coefficient of this coating is significantly higher, Figure 6.

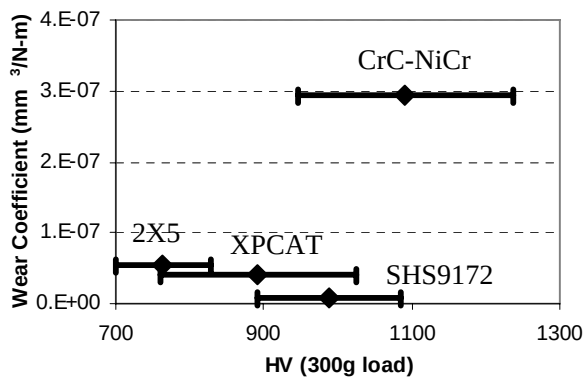

Figure 6 Volume loss vs. coating hardness

The best performing coating was the SHS9172 where the volume loss was hardly detectable, Figure 7a. The CrC-NiCr coating exhibited a significantly deeper wear scar compared to the fine grained/amorphous coatings, Figure 7d.

A closer examination of the worn surfaces indicated that the mechanisms responsible for wear were plastic ploughing and splat removal. The superior performance of the SHS9172 is demonstrated by the fact that the grinding marks from the specimen preparation are still present, to some extent, after the test, Figure 15a. Removal and fracture of splats from the coating is in particular evident in the amorphous SAM2X5 coating, Figure 15c. The predominant wear mechanism in the CrC-NiCr coating was plastic loss of binder and subsequent carbide removal, Figure 15d.

The average coefficient of friction (COF) of the coatings under the lubricated test condition ranged from 0.107-0.120. COF stabilized around the average value after about 1 hr of the test with the exception of the amorphous SAM2X5, Figure 16. It is unclear if this is a result of the material properties or particular test conditions. However, the large amount of splats pulled from the coating observed in the SAM2X5 surface morphology, Figure 15c, indicates that the hard splat debris between the pin and the coating may have caused the erratic COF.

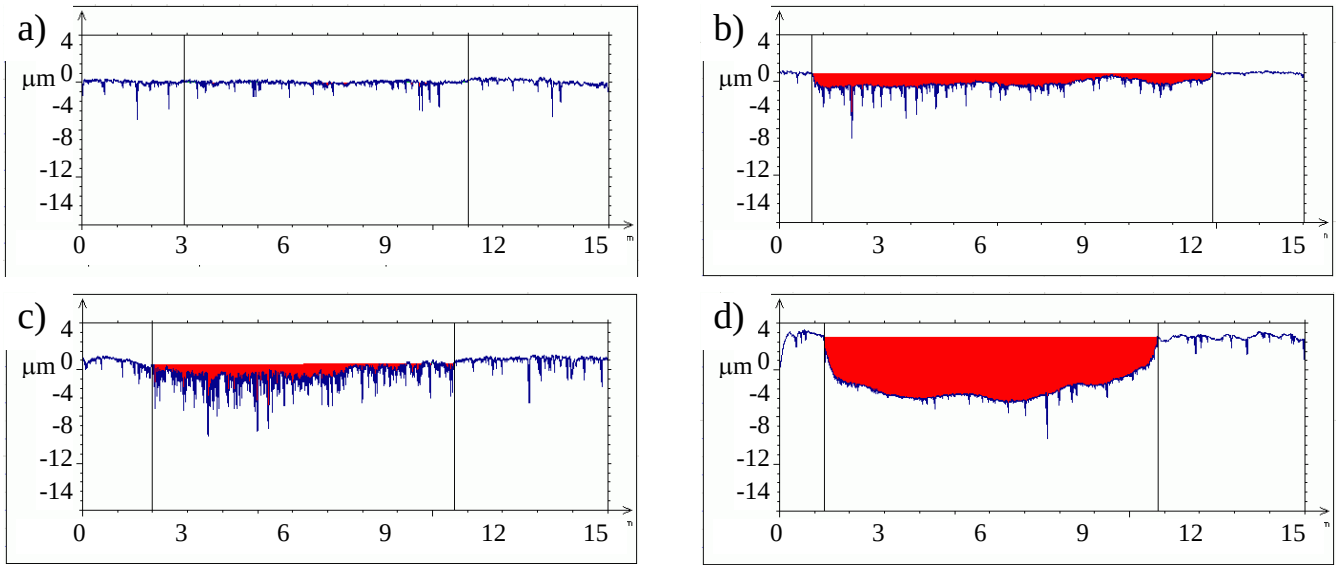

Figure 7 Cross sections of the wear scars; a) SHS 9172, b) CATXP, c) Amorphous SAM2X5, d) CrC-NiCr

Erosive wear resistance of SAM1651 and SAM2X5 coatings

The SAM1651 and SAM2X5 coatings were subject to erosion by alumina grit particles. A SAE 1045 steel heat treated to HRC 55 was used as a reference. A commercial grit-blasting unit was used to perform the test. The average grit particle size was approximately 700µm (mesh 24), pressure 60 PSI (4.14 bar), average media velocity 160-165 m/s. The blasting nozzle was traversed over the coating specimens at a constant speed of 100 mm/s. The change in coating thickness was measured.

The results indicate that the HVOF coatings perform worse under these conditions than bulk materials such as carbon steel, Figure 9. The SAM2X5 coating performed better than SAM1651, which indicates a better mechanical integrity of the SAM1651 microstructure.

The hardness of SAM coatings with the porosity and splat boundaries is in the 800-900 HV (300g) range, Figure 5. The hardness of the individual splats is probably similar to the hardness of amorphous as-spun ribbons, 1100 HV (100g) [2]. The lamellae in the HVOF coating microstructure are prone to delaminate, which increases the wear rate under impact conditions. However the wear surface exhibits more signs of plastic deformation, ploughing, rather than brittle cleavage, Figure 10.

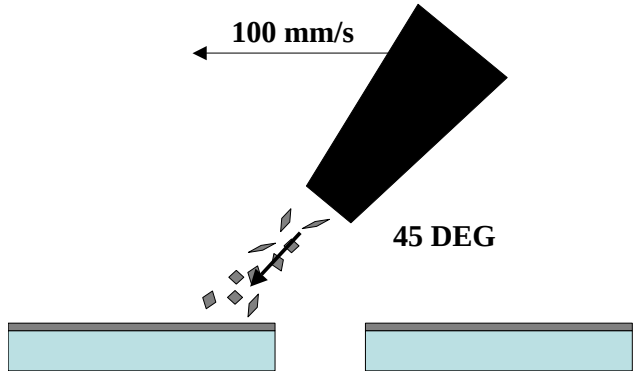

Figure 8 Experimental setup for the erosion test

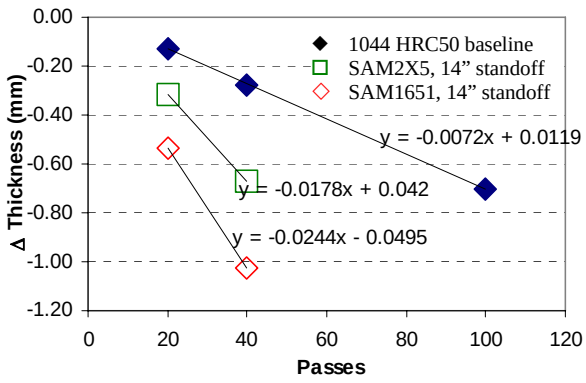

Figure 9 Erosion test results

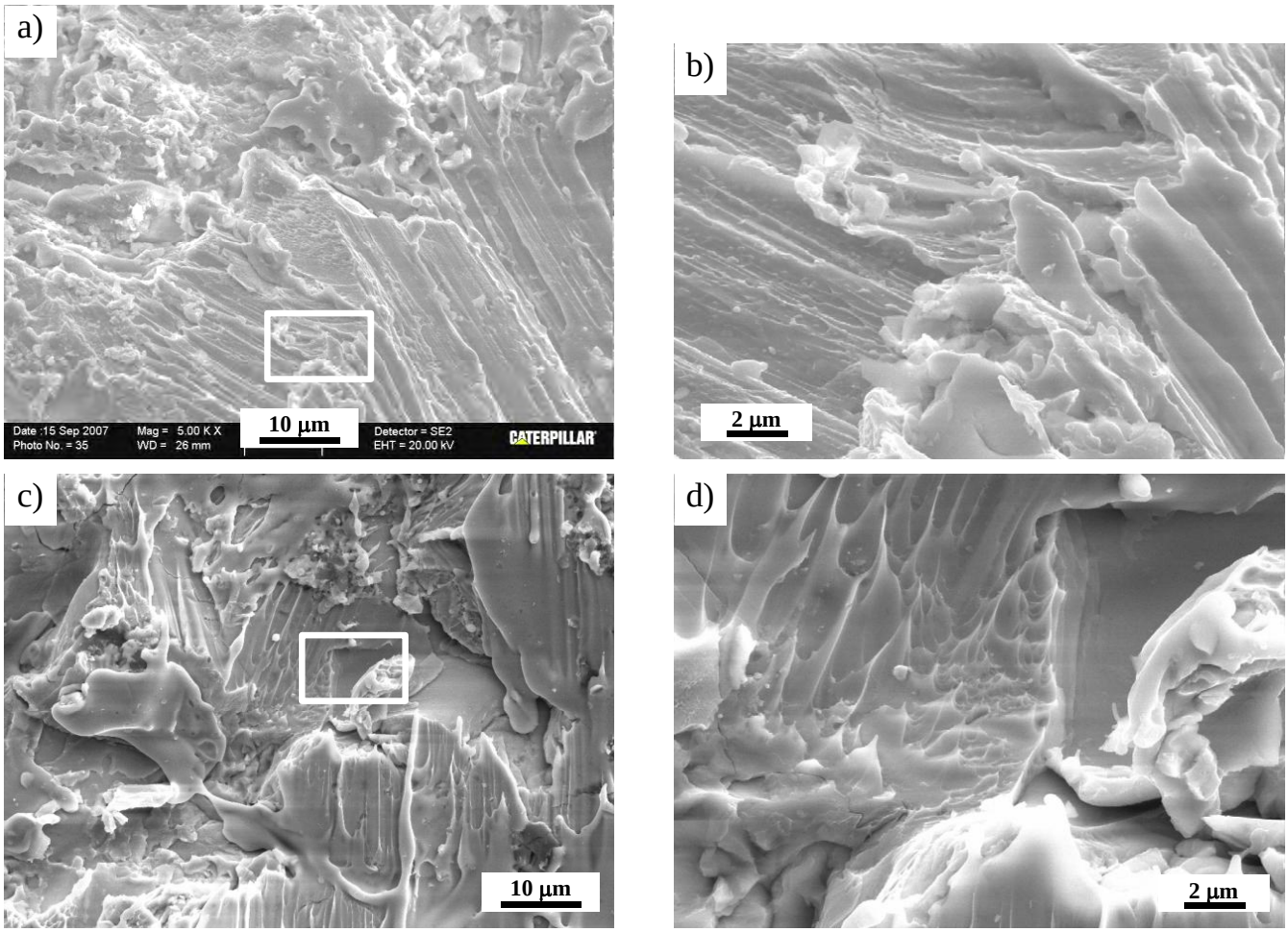

Figure 10 Surfaces of the coatings after erosive wear test; a) SAM2X5, b) SAM2X5 detail, c) SAM1651, d) SAM1651 detaiil

Tensile adhesion test

Tensile adhesion test was carried in a configuration described by ASTM C633 standard, Figure 11a. The SAM2X5 coatings performed better in adhesion than SAM1651. The SAM 2X5 coatings

generally exhibited delamination close to the substrate/coating interface; however, part of the fracture appeared within the coatings itself and finally between the adhesive compound and the counterpart, Figure 12a). The SAM 1651 coatings always exhibited the entire failure at the coating/substrate interface, Figure 12b).

Under a closer examination by means of scanning electron microscopy, it appears that even in the area where the coating failed close to the interface a thin layer of coating still adheres to the substrate, Figure 13. This indicates that the specimens failed mostly within the coating in a plane parallel to the substrate that crosses the peaks of grit blasted surface asperities and the peaks of the largest grit particles itself, Figure 14.

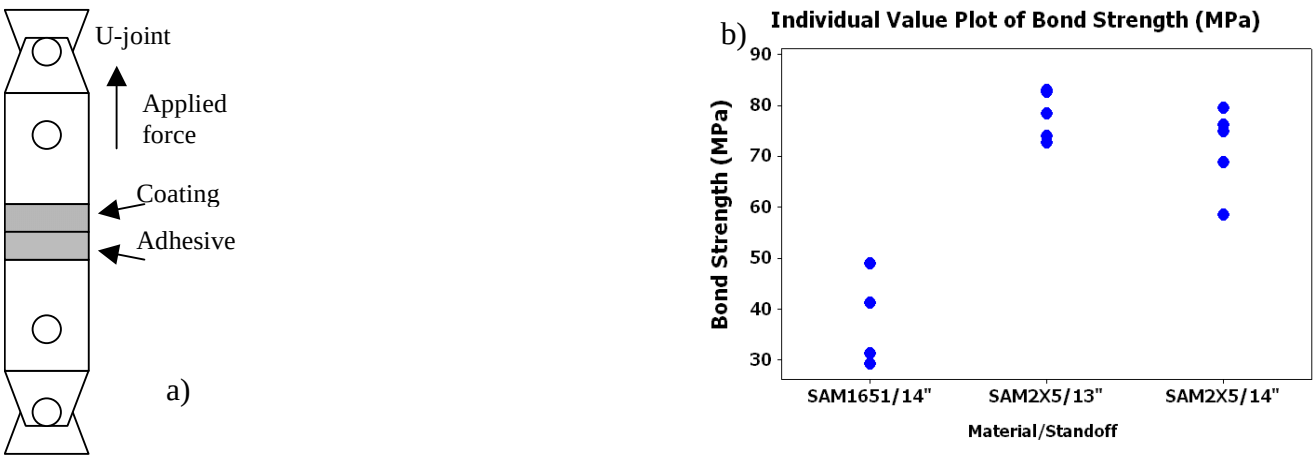

Figure 11 Bond strength of HVOF SAM coatings measured by tensile adhesion test (ASTM C-633); a) test setup, b) test results

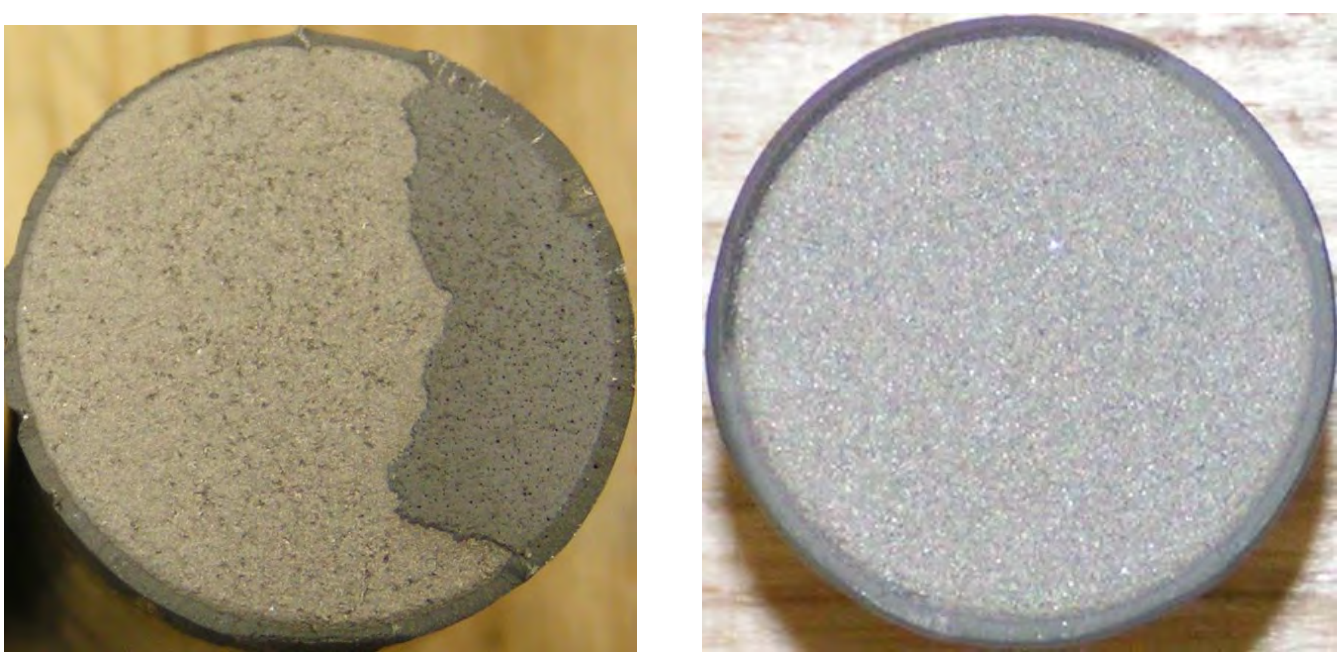

Figure 12 Failure modes of tensile adhesion specimens: a) SAM 2X5 mixed adhesion cohesion, b) adhesion

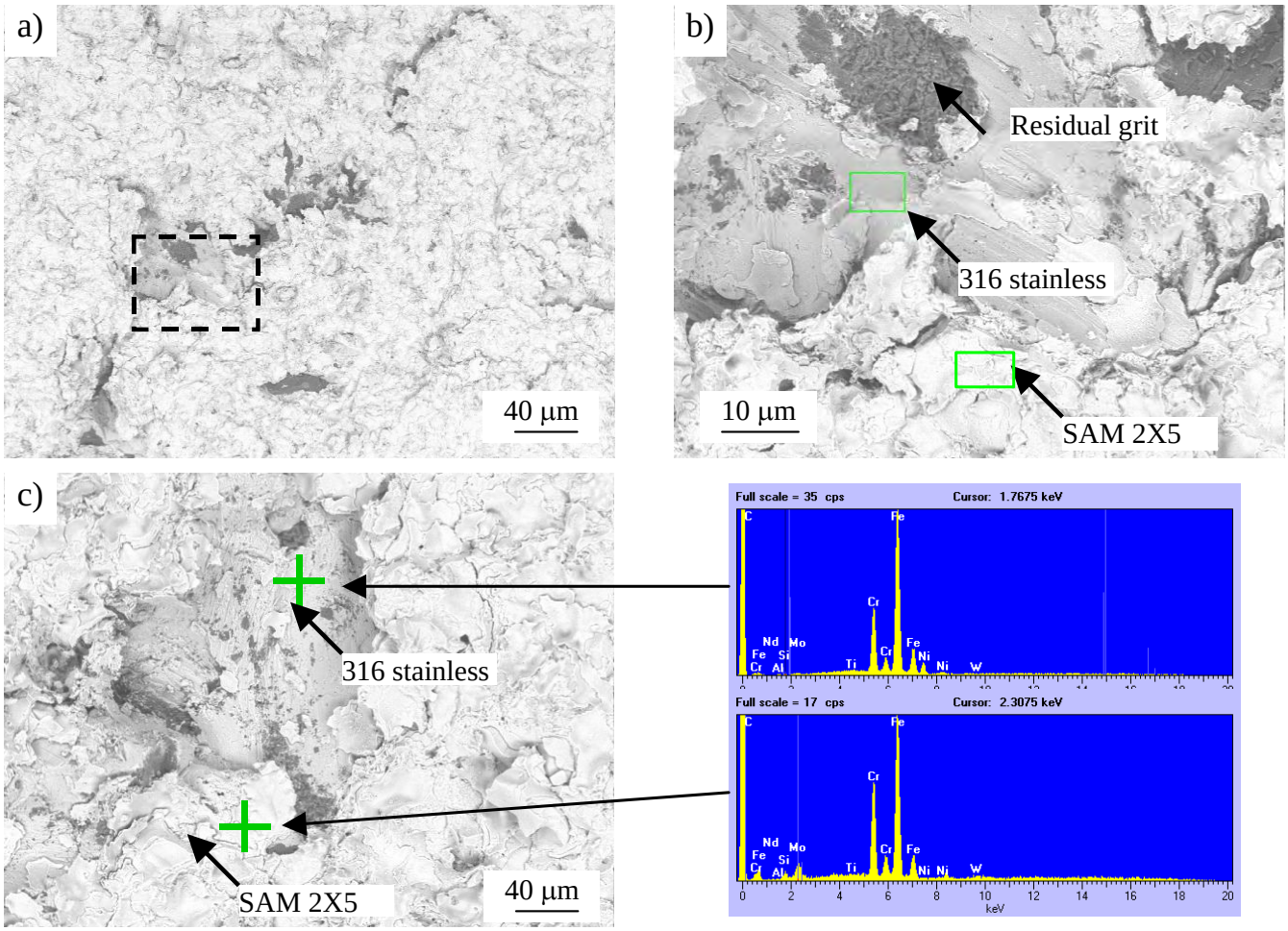

Figure 13 Tensile adhesion specimen substrate after the SAM2X5 coating has been removed during the test, a) overall view, b) detail of remaining coating, 316 stainless substrate, and residual grit, c) X-ray spectra

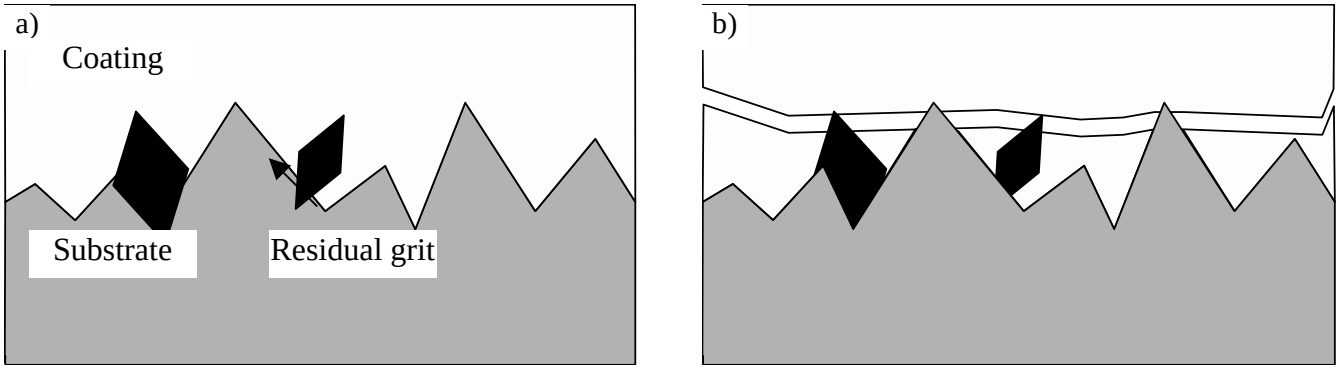

Figure 14 Propagation of a delamination crack, a) before test, b) after test

Instrumented indentation

The wear process consists of repeated loading of the material surface. It is assumed that the wear resistance of the material is related to the ability to restore the original dimension after a wear event such as scratch or indentation. To simulate the mechanical energy dissipation during a repeated wear event, the surfaces of the coatings were subjected to a Vickers indentation using a loading cycle with an increasing maximum load. The unloading curve is ideally elastic and repeated loading to the maximum force should follow the original unloading curve, however, reverse plasticity or other energy-dissipating mechanism leads to a hysteresis that can be measured by means of instrumented indentation.

The loading cycle was programmed to load the indenter with 3000, 6000, and 9000 mN. After 3000 and 6000 loads were reached the indenter was unloaded to 100mN before the next cycle. The area of hysteresis between the unloading and reloading branches at 3000 and 6000 mN, Figure 17a, was correlated with the wear coefficient of the coatings Figure 17b.

The plot reveals that the loading curve hysteresis is not a universal parameter indicating the wear coefficient because the hysteresis of the CrC-NiCr coating is comparable to the amorphous SAM2X5 coating, although the wear coefficient is considerably higher in case of Cr-NiCr. However, there is a monotonic relationship between the hysteresis and the wear coefficient within the class of fine-grained/amorphous materials. The CrC-NiCr coating is a very different system that consists of hard particles in a relatively soft matrix.

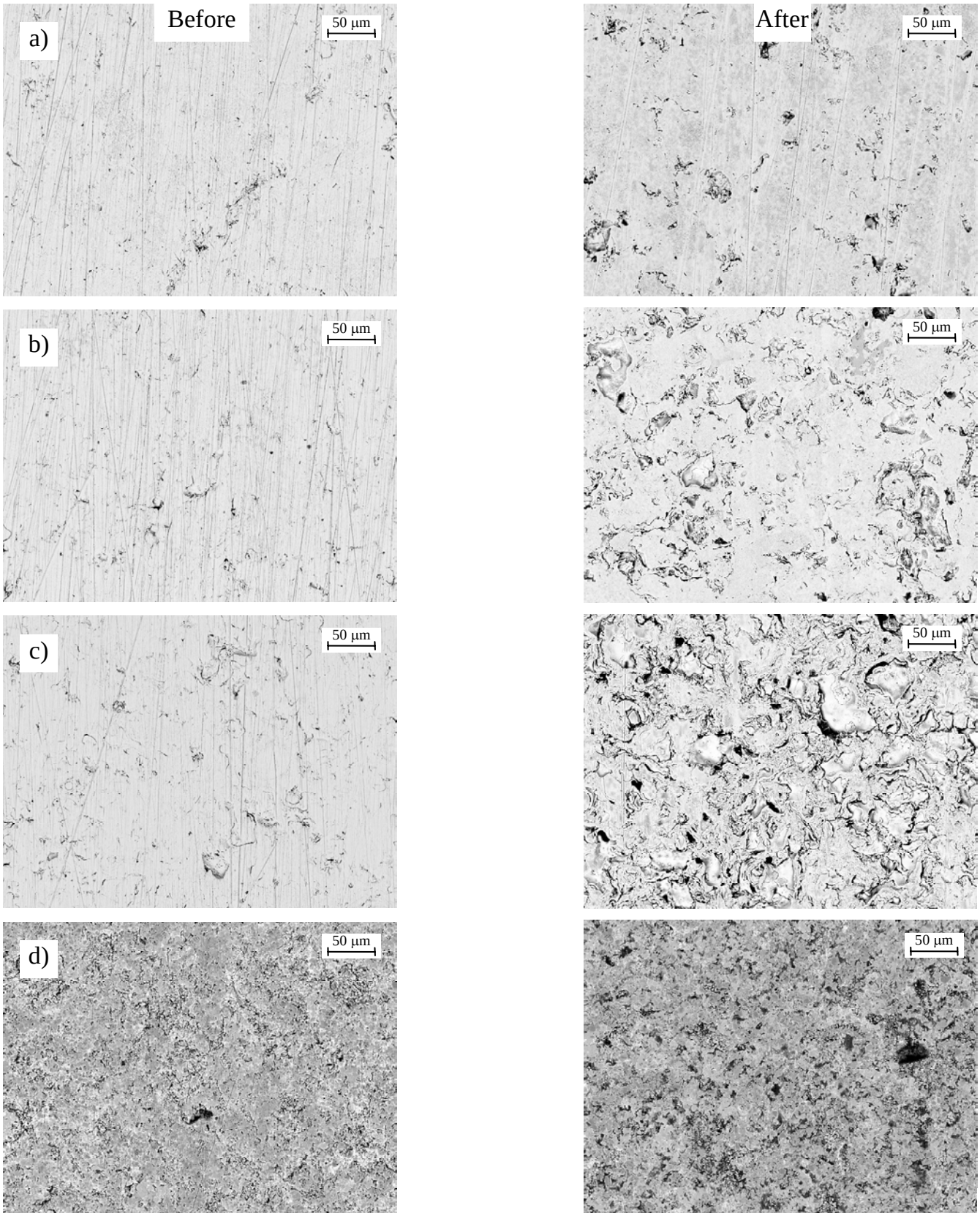

Figure 15 Specimen surface before and after wear test; a) SHS 9172, b) CATXP, c) Amorphous SAM2X5, d) CrC-NiCr

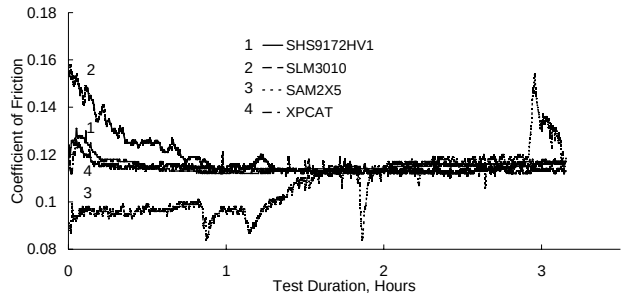

Figure 16 Coefficient of friction during the wear test

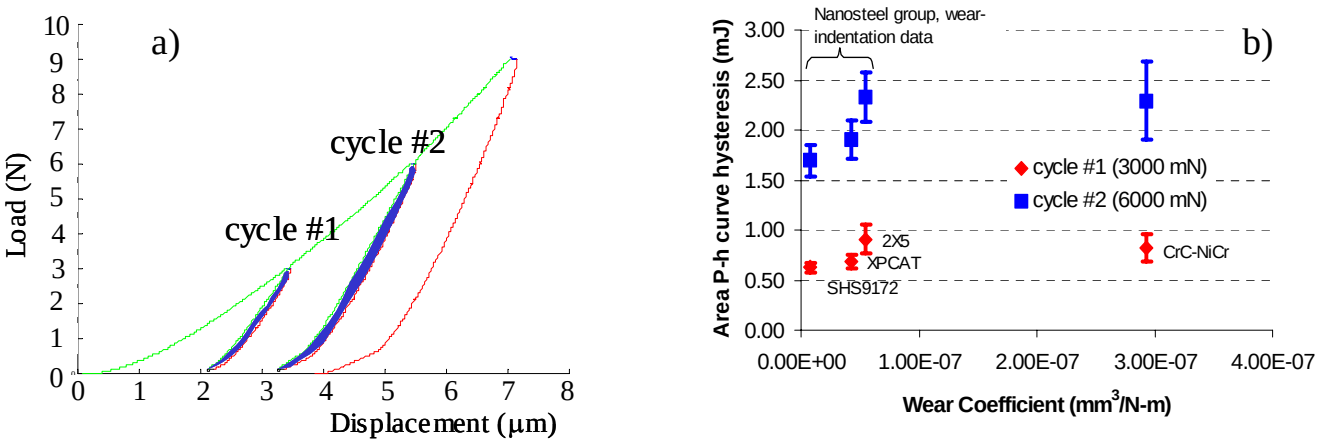

Figure 17 a) Load displacement curve with marked hysteresis areas of the unloading and loading branches, b) relation of the hysteresis and the wear coefficient

Discussion

The carbide cermet coatings consist of hard carbide phase distributed within a soft metal matrix. Matrix removal and failure of the carbide-matrix bond are the likely wear mechanisms in these coatings. Unlike the cermet coatings, a high hardness phases or their mixtures are present throughout the microstructure of the fine-grained/amorphous materials, which results in a higher wear resistance of these coatings. The predominant wear mechanisms are ploughing, splat boundary fracture and splat removal.

The amorphous coating appears to be the coating most prone to removal and/or fracture of splats, which act as abrasive when dispersed in the lubricant. The hardness and wear resistance of the amorphous SAM2X5 coating can be expected to increase with heat treatment to produce more nanocrystalline phase [3].

Shear stress in sliding contact causes plastic deformation that results in energy dissipation and subsequent damage. The damage may result in crack nucleation and propagation [9]. The inter-splat boundaries in thermal spray coatings act as pre-existing cracks that facilitate the splat removal. Indentation data can be analyzed with respect to energy accumulated in the material during a loading cycle and it is hypothesized that there is a relationship to the wear coefficient. The mechanism causing the indentation loading-unloading curve hysteresis may be related to reverse plasticity or splat sliding. Reverse plasticity may be expected close to the tip of a Vickers indenter; however, for example no reverse plasticity was found through finite element modeling (FEM) on aluminum alloys [12]. The relationship of the indentation curve hysteresis and the wear coefficient indicates that similar

mechanism, cyclic plasticity, is demonstrated in both the sliding wear test and the indentation test. However, the relationship is not applicable when comparing the cermet and nano-composite materials, which is likely due to a different wear mechanism.

It should be noted that the specimens tested in sliding wear had various amount of porosity on the machined surface, which may have affected the wear and coefficient of friction. Coating porosity can retain the lubricant and therefore is beneficial for sliding wear resistance under lubricated condition [15]. On the other hand splat boundaries and porosity lower the coating strength. Erosion of thermal spray coatings may be dominated by separation of thin splats, which increases the wear rate. The observation in the present study correlates with published results of other authors. For example, mild steel with hardness less than 200HV(25g) was reported to have a higher erosion resistance than plasma sprayed CrC-NiCr coating with hardness more than 800HV(25g) [16]. Sintered 83WC-17Co was several times more erosion-resistant than a HVOF coating made of the same composition [17]. The difference between erosion resistance of a sintered and thermal spray materials increases with the impact energy [18].

SAM2X5 coatings performed better in the tensile adhesion test. It appears that at least a part of the failure occurs within the first layer of coating at the coating/susbtrate interface and therefore is controlled by the cohesion of the splats. This result is in agreement with a better SAM2X5 performance in the erosion test where the wear mechanism is dominated by splat removal.

Conclusions

The present study demonstrates promising wear properties of amorphous and fine-grained materials that are derived from formulations developed to posses low critical cooling rate. These materials have a potential to perform better in sliding wear under lubricated conditions than currently used carbide cermets. It should be noted that tungsten carbide (WC) coatings that generally have higher hardness were not investigated. Coatings that contain tungsten carbide may perform well in some applications such as abrasion and erosion wear [13]. However, in other studies, e.g. dry and lubricated pin on disk test [14], the wear resistance of chromium carbide coatings is better.

Further development, specifically HVOF parameters optimization, will address the coating porosity and oxide content.

Acknowledgements

This work supports the High Performance Corrosion-Resistant Materials (HPCRM) program sponsored by Defense Advanced Projects Agency (DARPA), Defense Science Office (DSO) and the Department of Energy (DOE) Office of Civilian Radioactive Waste Management (OCRWM).

References

[1] Farmer, J.C., et al. *Corrosion characterization of iron-based high-performance amorphous-metal thermal-spray coatings*. 2005. Denver, CO, United States: American Society of Mechanical Engineers, Pressure Vessels and Piping Division (Publication) PVP, 7, American Society of Mechanical Engineers, New York, NY 10016-5990, United States 583-589.

[2] Branagan, D.J. and Y. Tang, *Developing extreme hardness (>15GPa) in iron based nanocomposites.* Composites - Part A: Applied Science and Manufacturing, 2002. **33**[6], 855-859.

[3] Branagan, D.J., et al., *Wear-resistant amorphous and nanocomposite steel coatings.* Metallurgical and Materials Transactions A: Physical Metallurgy and Materials Science, 2001. **32**[10], 2615-2621.
[4] Poon, S.J., et al., *Synthesis of iron-based bulk metallic glasses as nonferromagnetic amorphous steel alloys.* Applied Physics Letters, 2003. **83**[6], 1131-1133.
[5] Wang, Y., et al., *High tensile ductility in a nanostructured metal.* Nature, 2002. **419**[6910], 912-915.
[6] Wolf, D., et al., *Deformation of nanocrystalline materials by molecular-dynamics simulation: Relationship to experiments?* Acta Materialia, 2005. **53**[1], 1-40.
[7] Jia, K. and T.E. Fischer, *Abrasion resistance of nanostructured and conventional cemented carbides.* Wear, 1996. **200**[1-2], 206-214.
[8] Stewart, D.A., P.H. Shipway, and D.G. McCartney, *Abrasive wear behaviour of conventional and nanocomposite HVOF-sprayed WC-Co coatings.* Wear, 1999. **229**, 789-798.
[9] Fouvry, S., P. Kapsa, and L. Vincent, *Quantification of fretting damage.* Wear, 1996. **200**[1-2], 186-205.
[10] Cheng, F.T., P. Shi, and H.C. Man, *Correlation of cavitation erosion resistance with indentation-derived properties for a NiTi alloy.* Scripta Materialia, 2001. **45**[9], 1083-1089.
[11] Branagan, D.J., M.C. Marshall, and B.E. Meacham, *High toughness high hardness iron based PTAW weld materials.* Materials Science and Engineering A, 2006. **428**[1-2], 116-123.
[12] Giannakopoulos, A.E., P.-L. Larsson, and R. Vestergaard, *Analysis of vickers indentation.* International Journal of Solids and Structures, 1994. **31**[19], 2679-2708.
[13] Legoux, J.G., S. Bouaricha, and P. Marcoux. *Abrasion and erosion behavior of WC and CrC cermet coatings*. 2004. Osaka, Japan: Proceedings of the International Thermal Spray Conference, ASM International, 9639 Kinsman Road, OH 44073-0002, United States 1040-1045.
[14] Forn, A., J.A. Picas, and G. Matthaus. *Wear behaviour of HVOF thermal sprayed WC-Co and CrC-NiCr coatings*. 2003. Madrid, Spain: Materials Science Forum, 426-432, Trans Tech Publications Ltd 2623-2628.
[15] Ilyuschenko, A., et al. *Investigation of Composite Powders with a Carbide Phase for Plasma Spraying of Wear Resistant Coatings*. 2001. Singapore, Singapore: Proceedings of the International Thermal Spray Conference, ASM International 1119-1122.
[16] Sonoya, K. *Blast Erosion Properties of Erosion-Resistant Thermally Sprayed Coatings*. in *Thermal Spray 2001 New Surfaces for a New Millennium: Proceedings of the International Thremal Spray Conferences, May 28-30 2001*. 2001. Singapore, Singapore: Proceedings of the International Thermal Spray Conference, ASM International 1303-1311.
[17] Akasawa, T. and K. Ai. *Wear properties of WC/Co coatings with plasma and high velocity oxyfuel spraying*. 1998. Nice, France: Proceedings of the International Thermal Spray Conference, 1, ASM International 281-286.
[18] Wood, R.J.K., B.G. Mellor, and M.L. Binfield, *Sand erosion performance of detonation gun applied tungsten carbide/cobalt-chromium coatings.* Wear, 1997. **211**[1], 70-83.

This work performed under the auspices of the U.S. Department of Energy by Lawrence Livermore National Laboratory under Contract DE-AC52-07NA27344.